

SCIENTIFIC REPORTS

OPEN

The Molecular Dynamics Study of Vacancy Formation During Solidification of Pure Metals

H. Y. Zhang^{1,2}, F. Liu¹, Y. Yang¹ & D. Y. Sun¹

In order to understand the defect trapping during solidification in pure elements, we have performed molecular dynamics simulations on both aluminum and nickel. We find that vacancies are the dominant defects in the product crystals for both metals. For slight undercooling, the vacancy concentration strongly depends on the growth velocity, rather than the growth orientations, and there is an approximately linear relationship between the growth velocity and vacancy concentration. However, for deep undercooling, the vacancy concentration shows a remarkable anisotropy between (100) and (110) orientations. Based on the competition between atomic diffusion and growth, a possible mechanism for vacancy trapping is suggested.

In the last couple of decades, computer simulations have been extensively applied on the solidification of metals^{1,2}. Up to date, the significant progress in understanding the solidification kinetics has been achieved on pure metals^{3–36} and a few binary alloys^{37–41}. Despite the advances, one of the final pieces, namely the defect trapping during solidification, remains less investigated^{42–51}. There are at least two reasons making this topic significant. First, the defect concentration may play an important role in determining the quality of the final solidification product. Second, the quantitative understanding of defect trapping continues to pose a major theoretical challenge.

There have been a few molecular dynamics (MD) studies on defect or solute trapping during solidification. Most of these studies have focused on alloys. For example, Zheng *et al.* have reported the obvious defect trapping including the formation of both antisite and vacancy in the crystallization of NiAl alloy³⁹. Kramer, Mendeleev and Napolitano have investigated the defect generation in the rapid solidification of the Zr₂Cu compound⁴⁰. Yang *et al.* have studied the solute trapping behavior for a Lennard-Jones model alloy⁴¹. However, the defect trapping in solidification process of pure elements is still less explored. The atomic mechanism of defect trapping, as well as its dependence on growth velocities and/or undercooling (defining as $\Delta T = T_M - T$, T_M is the melting point) remains unclear. In this study, we take Ni and Al as typical examples to investigate the defect trapping behaviors during the solidification process.

Based on the current calculations, it is interesting to find that, only one type of point defects, namely the vacancy, is observed. The vacancy concentration not only depends on interfacial velocities but also depends on growth orientations at deep undercooling. However, at slight undercooling, the vacancy concentration seems to be only related to growth velocities.

Results and Discussions

Figure 1 plots the interfacial velocity as a function of temperature for both Ni (upper panel) and Al (lower panel). The error bars in interface velocities denote the standard errors in the mean value of interface velocity, obtained from the variance of the interface velocity derived separately from each of independent simulations for a given temperature. The interface velocities obey a linear relationship as a function of temperature in the range of small undercooling (ΔT). The constant of proportionality between interface velocities and temperature is the kinetic coefficient (μ), which characterizes the crystal-melt interfacial mobility. The present results for μ are listed in Table 1, which are in good agreement with the previous results^{29,31}.

When the systems are cooled further, the interface velocity continues to increase until it reaches a maximum. A temperature (T^*), at which the interfacial velocity reaches the maximum, is defined. T^* is indicated by arrows in Fig. 1, also listed in Table 1. It is interesting to find that, the growth velocity shows significant different temperature dependence between $T > T^*$ and $T < T^*$. For $T > T^*$, the growth velocity monotonically

¹Department of Physics, East China Normal University, Shanghai, 200062, China. ²Physical Science and Technology College, Yangzhou University, Yangzhou, 225002, China. Correspondence and requests for materials should be addressed to D.Y.S. (email: dysun@phy.ecnu.edu.cn)

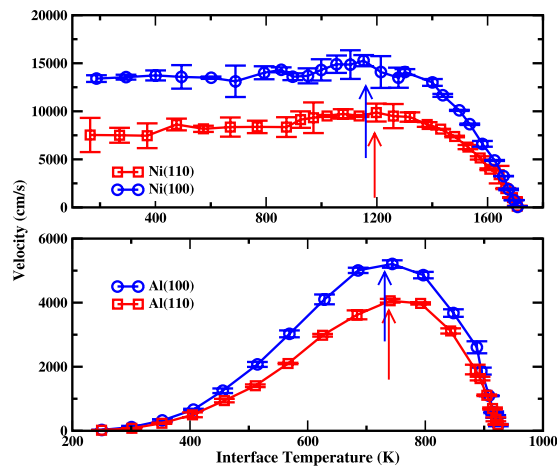


Figure 1. The crystal-melt interface velocity as a function of temperature for Ni (upper panel) and Al (lower panel). The arrow marks the temperature (T^*), at which the interfacial velocity reaches the maximum.

	Orientation	μ ($ms^{-1} K^{-1}$) (refs 29, 31)	μ ($ms^{-1} K^{-1}$) (This work)	T^* (K)
Ni	(100)	0.71	0.66 ± 0.11	~ 1160
Ni	(110)	0.50	0.44 ± 0.04	~ 1192
Al	(100)	0.68	0.60 ± 0.23	~ 730
Al	(110)	0.59	0.48 ± 0.11	~ 738

Table 1. Values for the kinetic coefficient (μ) along (100) and (110) growth orientations of Ni and Al. The last row lists the temperature (T^*), at which the interfacial velocity reaches the maximum.

increases with the decrease of temperatures, while it keeps no increase as the undercooling decreasing at $T < T^*$. The velocity-temperature curves for both Ni and Al, either (110) or (100) orientations, are similar at $T > T^*$. When the temperature is below T^* , the velocity-temperature curve becomes much different between Ni and Al. Namely, with the decrease of temperature the velocity almost keeps constant for Ni, while for Al the velocity begins to decrease dramatically and decline to zero around 200 K. In the whole range of temperatures, the growth velocity of (100) orientation is always larger than that of (110) orientation for both Al and Ni. Our results are consistent with the general trends found in metals so far, and the velocity-temperature curve of Al and Ni represents two typical solidification processes in pure metals^{26, 30, 36}.

The significant difference between Ni and Al at $T < T^*$ mentioned above may stem from the structural character of liquids. It has been found that, liquid Al with the current potential is more ordered than liquid Ni^{31, 32}. However, the difference could be complicated and related to many factors. Indeed the growth velocity-temperature curve of Al and Ni is not isolated incident, which is also found in other metals^{26, 30, 36}. Since our interests in current work is the defect trapping during the solidification, the issue regarding the growth mechanism and anisotropy will not be discussed further.

The point defects are observed at all the studied systems and temperatures. The dominated defect is the vacancy, but free of the interstitial. Even at the deep undercooling, only vacancies are observed. Figure 2 presents a few snapshots of lattice plane in the product crystal. We find that most vacancies are isolated. Only in a few cases, a pair of vacancies are formed (see Fig. 2(c)) but with an extremely low probability. Few vacancy clusters (including more than three vacancies) are observed.

The vacancy concentration as the function of interface temperature is depicted in Fig. 3. A few features can be seen from this figure. (1) Vacancy concentrations increase with the increase of undercooling in the whole range of temperature, which is much different from the growth velocity (Fig. 1). (2) A prominent anisotropy between (100) and (110) orientations for both metals is observed, and the vacancy concentration for (100) orientation is always larger than that of (110) orientation at the same temperature. (3) The vacancy generation is dependent on materials. The concentration of vacancies in Al is higher than that in Ni.

From Fig. 3, we can find another interesting feature. The concentration-temperature curves can be roughly viewed as two straight lines meeting at T^* . The slope of the straight line for $T > T^*$ is slightly larger than that for $T < T^*$. This feature is much evident in Al(100) orientations. As mentioned above, around T^* , the growth mechanism may change. The current results indicate that the growth mechanism could affect the disorder trapping. In turn, the disorder trapping may also affect growth mechanism. Although how the growth affecting the generation of vacancies remain unclear (we have proposed a possible mechanism in current work (see below)), the effect of vacancies on the growth is understandable, at least partially. With the increase of the vacancy concentration in solid phases, the free energy difference between solid and liquid will decrease, thus the driving force for the solidification (the free energy difference between solid and liquid phase) will be reduced accordingly.

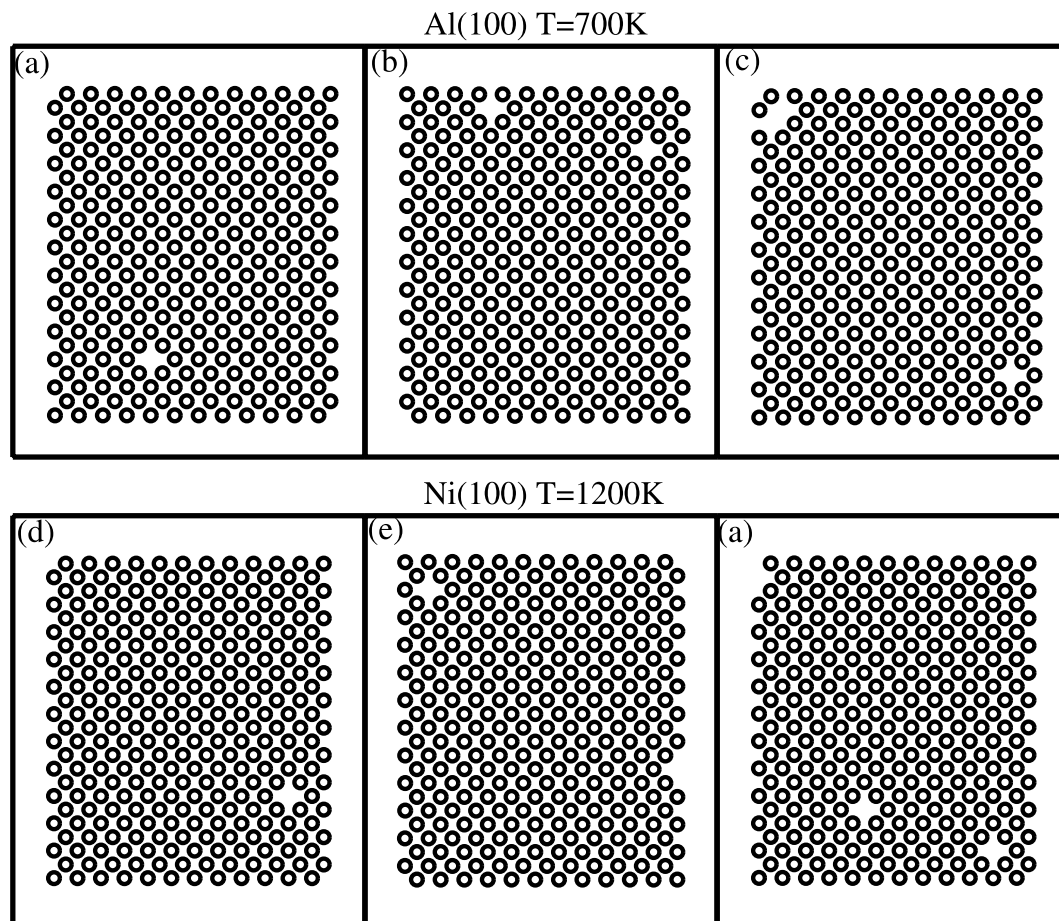


Figure 2. Snapshots of a few selected crystal planes after the solidification for Al(100) orientation (upper panel) and Ni(100) orientation (lower panel).

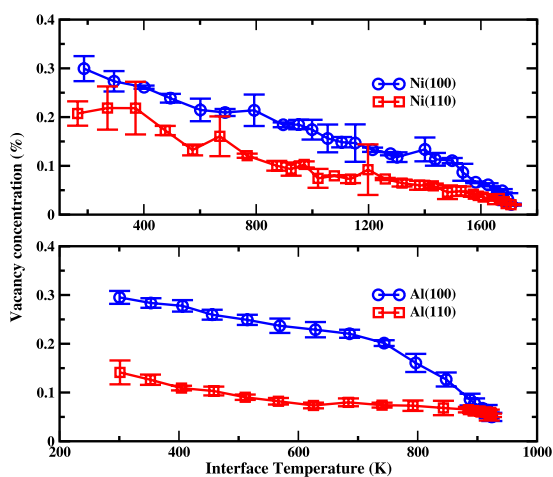


Figure 3. The concentration of vacancies in product crystal of Ni (upper panel) and Al (lower panel) as a function of interfacial temperatures.

Thermodynamically, point defects should always exist in a crystal above zero temperature. According to the data shown in Fig. 3, we could safely attribute the generation of vacancies mainly to the the rapid solidification of liquid, rather than the equilibrium thermodynamics effect. At least four facts support this interpretation. First, one can see that the vacancy concentration increases with the decrease of temperatures. If the vacancy concentrations correspond to thermodynamics equilibrium concentration of vacancies (TECV), it will show the opposite behavior, *i.e.*, decreasing concentration with decreasing temperature. Second, the existence of the remarkable

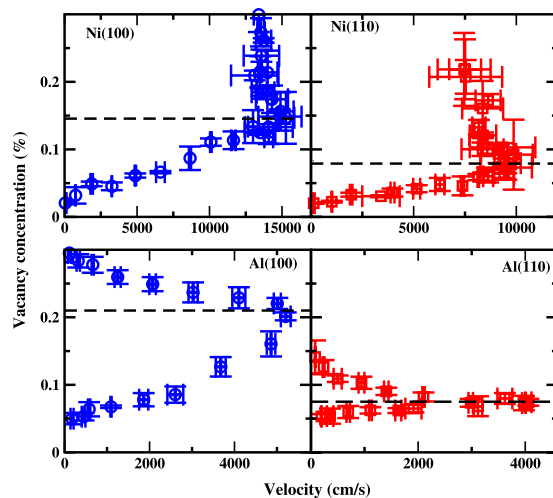


Figure 4. The concentration of vacancies in product crystal of Ni (upper panel) and Al (lower panel) as a function of interface velocities. The horizontal dash lines pass the maximum interfacial velocity. Below (above) the dash line, $T > T^*$ ($T < T^*$).

anisotropy indicates non-TECV character, since at thermodynamics equilibrium, the concentration of vacancies should not be correlated to growth directions. Third, according to the formation energy of vacancies in Al (0.69 eV)⁵² and Ni (1.63 eV)⁵³, TECV of Al should be much higher than that of Ni at the same temperature. However as shown in Fig. 3, the vacancy concentrations between Al and Ni do not show much difference at the same temperature. At last, the vacancy concentrations shown in Fig. 3 are significantly larger than TECV (0.0016% and 0.02% for Ni and Al at melting temperature, respectively) calculated basing on the formation energy quoted above.

In Fig. 4, we have shown vacancy concentrations via interface velocities for both Al and Ni. Although Fig. 4 is a re-packaging of the data in Figs 1 and 3, it does contain more information, which is hard to see from both Figs 1 and 3. One remarkable feature is that, the vacancy concentration is not single valued function of interfacial velocities. Data presented in Fig. 4 can be divided into two parts according to the temperature above or below T^* , which is indicated by a horizontal dash line. For the lower part (below the horizontal dashed line in Fig. 4), where the temperature is higher than T^* , the vacancy concentrations increase with the increase of interface velocities. In this part, there is no significant anisotropy between (100) and (110) orientations for small growth velocities, which is similar to the disorder trapping observed in NiAl alloy³⁹. For another part (above the dashed line in Fig. 4), corresponding to the deep undercooling region ($T < T^*$), the opposite situation is observed, namely as the interface velocity increases, the anisotropy becomes more and more significant. The unexpected dependence of vacancy concentrations on interface velocities implies that, besides of growth velocities, there are other important facts strongly affecting the generation of vacancies. Future understanding of solidification process may require the knowledge of both defect trapping and growth mechanism.

Although the mechanism for vacancy trapping in pure metals remains unclear up to date, it is still possible to give a constructive discussion based on current results. As we have discussed above, for vacancy trapping, the kinetics rather than thermodynamics may play the leading role. In the viewpoint of kinetic effects, the crystal growth and atomic diffusion should be the major processes responding to the generation of vacancies. On the one hand, the crystallization process solidifies a disordered melt into an ordered crystal around the solid-liquid interface. This process can be imagined to *eliminate* liquid atoms at the interface. On the other hand, the diffusion process carries liquid atoms into the interface. Thus the competition between diffusion and growth could affect the production of vacancies. It is reasonable to speculate that the ratio between the diffusion flux and growth rate could play a role in the generation of vacancies. If the diffusion prevails, less vacancy will be expected. If diffusion does not prevail, then more vacancy should be expected.

To characterize the competition between atomic diffusion and growth process, we have defined a quantity $R \left(R = \left| \frac{J_D}{J_G} \right| \right)$, which describes the ratio between the diffusion flux (J_D) and growth rate (J_G). J_D is defined as the number of atoms passing the solid-liquid interface per unit time. According to Fick's first law, we have, $J_D = -D \Delta n$, where D and Δn are the diffusion constant and atomic density gradient, respectively. $\Delta n = \frac{\rho_s - \rho_l}{d}$, where ρ_s and ρ_l are the density of solid and liquid phase respectively, and d refers to the effective interfacial width. According to previous studies^{12, 54}, an effective interfacial width can be approximately as three atomic layers, irrespective of the crystal orientation. In current work, d is taken as three times interfacial spacing. Similarly, we can define a growth rate, which characterizes the number of atoms *eliminated* through the solid-liquid interface per unit time. Thus, $J_G = V(\rho_s - \rho_l)$, where V is the interfacial velocity. Finally, we have $R = \left| \frac{J_D}{J_G} \right| = \left| \frac{D}{Vd} \right|$.

As shown in Fig. 5, the positive correlation between the vacancy concentration and R can be found. From this figure, one can see that, with the increase of R , the vacancy concentration decreases monotonically. At large R , in which the atomic diffusion process is faster than the growth process, the concentration of vacancies is less. On

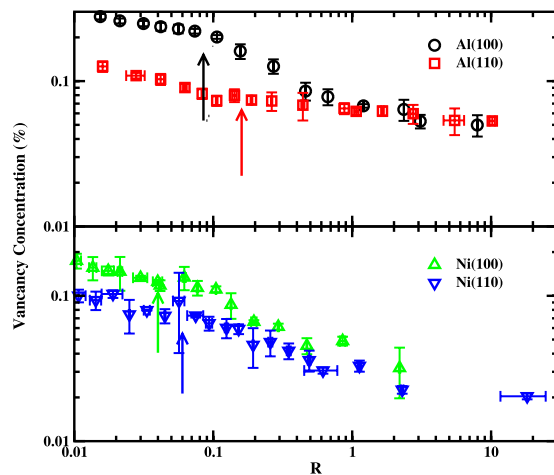


Figure 5. The concentration of vacancies as a function of R (the ratio between the diffusion flux and growth rate). The arrow marks T^* .

the contrast, the growth rate surpasses diffusion flux when R is small, which is conducive to trap more vacancies. Similar to concentration-temperature curves, Fig. 5 can also be roughly viewed as two straight lines (in log-log plot) cross around T^* (indicated by arrows). At $T < T^*$, the change of vacancy concentrations with R is slower than that at $T > T^*$. Although Al and Ni have much different growth behavior (see Fig. 1), the concentration- R curve shown in Fig. 5 is much similar to each other. As mentioned above, for the rapid solidification, a well-accepted theoretical or predictive model is still not available. The current study would shed light on both growth mechanism and disorder trapping.

At last, it is interesting to compare current results with that for B2 (CsCl prototype) ordered NiAl compound³⁹. Similar to pure Ni and Al presented here, the vacancy is also one of the dominant defects in ordered NiAl compound. At a given growth velocity, the magnitude of the vacancy concentration in NiAl alloy is much larger than that of pure Al and Ni, which may stem from the different growth mechanism. What more, at small undercooling, similar to NiAl alloy, the vacancy concentration mainly depends on growth velocity, regardless of orientations.

In conclusion, our theoretical calculations demonstrate that, during the process of solidification, the notable vacancies is produced for both metals. For slight undercooling, the vacancy concentration is mainly dependent on the growth velocity, but weakly dependent on the interfacial orientation. For deep undercooling, the vacancy concentration does not solely depend on the growth velocity, but also shows a strong anisotropy behavior. Finally, based on the ratio between the diffusion flux and growth rate, a possible mechanism for the vacancy generation is also proposed. The present results could prompt people to re-evaluate the current model for solidification based on the kinetic attachment, and re-check the role played by the atomic diffusion.

Methods

The MD simulations are performed by LAMMPS (large-scale atomic/molecular massively parallel simulator) code⁵⁵. All simulations take a time step of 1 fs. Temperature and pressure of systems are controlled by using a Nose'-Hoover thermostat^{56,57} and Parrinello-Rahman barostat^{58,59}, respectively. The pressure of the system is kept at ambient pressure (1 bar). The many-body potential developed by Foiles *et al.*⁵³ and by Ercolessi *et al.*⁵² are adopted for Ni and Al, respectively. Both potentials have been used to investigate the solidification process previously^{23,29-31,60,61}.

In order to set up proper simulation cells, the lattice constant as a function of temperature is calculated. Then the melting temperature, determined by using the modified coexistence approach²³, is estimated around 939 K and 1710 K for Al and Ni respectively, which is in good agreement with the previous results^{23,31}. The simulation cells are established by taking a rectangular crystal of fcc Ni and Al crystal. The z direction is perpendicular to the solid-liquid interface, while the x and y directions are parallel to the solid-liquid interface. Periodic boundary conditions are used along three directions. The initial system for solidification simulations roughly containing 20% crystal and 80% liquid is equilibrated at melting temperatures. In order to guarantee the reliability of simulation results, the system has been set to have large cross-sectional area ($A = L_x \times L_y$) and very long length in z direction (L_z). Two orientations, fcc (100) and fcc (110) of Ni and Al are considered in current studies. A $12 \times 12 \times 76$ supercell including about 80640 atoms and a $8 \times 12 \times 84$ supercell containing around 75264 atoms are used for (100) and (110) orientations, respectively.

The solidification simulations are performed under NP_zAT ensemble, the total number of atoms (N) and the cross-sectional area (A) are fixed, the length of the simulation cell perpendicular to the interfaces (L_z) is dynamic to maintain constant pressure normal to the interface²². Since the length of systems in current calculations is much longer (about 60 nanometers), the self-interaction among the periodic images of interfaces can be safely neglected according to the previous studies. Non-equilibrium MD simulations start from the initial two phase coexistence configurations at T_M , run under $T < T_M$ with A being scaled to let crystal structure matching pre-calculated lattice constant at the given T . Figure 6 shows a snapshot illustrating the two-phase equilibrium state of the system, used as a starting point for subsequent non-equilibrium MD solidification simulations. To

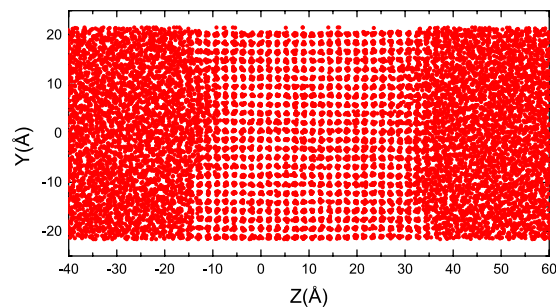


Figure 6. A snapshot of an initial equilibrium state used for subsequent solidification simulations (atoms only around solid-liquid interfaces are shown). Note, there are two crystal-melt interfaces in one periodic simulation cell.

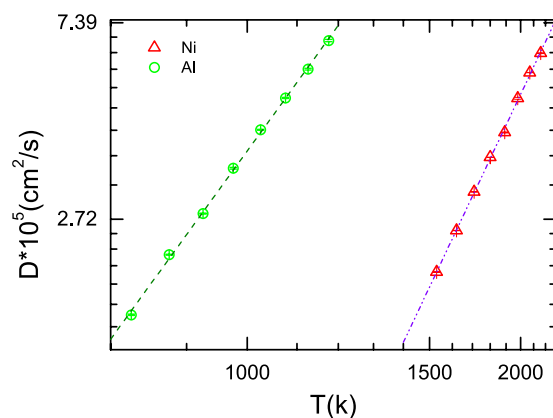


Figure 7. Diffusion constants versus temperature for Al (green circles) and Ni (red triangles), where the y-axis is logarithmic and the x-axis is reciprocal temperature. The dotted-dashed lines (Ni) and dashed lines (Al) are the Arrhenius fit to the data.

ensure reliable statistics, a few independent simulations are carried out at each undercooling. To track interfacial positions, an order parameter is calculated over narrow bins oriented parallel to the solid-liquid interface, and analyzed as a function of distance along the interfacial normal. The interfacial position thus is defined as the largest jump in order parameter. The order parameter is defined as, $\phi_i = (1/N_n) \sum_j |r_{ij} - r_{ij}^{ideal}|^2$, where the sum extends over the N_n nearest neighbors, r_{ij} is the vector connecting sites i and j and r_{ij}^{ideal} is the corresponding vector in an ideal crystal. For fcc crystal, $N_n = 12$. More details about the order parameter and the determination of interfacial position are referred to the work of Hoyt *et al.*⁶² and Sun *et al.*²².

Recent studies^{29, 31, 34, 39, 41} have shown that during non-equilibrium molecular dynamics simulations of solidification, the generation of latent heat at the moving solid-liquid boundary could lead to the formation of large temperature gradients around solid-liquid interfaces, which results in the interfacial temperature being different from the thermostat temperature. To obtain the true interface temperature, the temperature profiles along the interfacial normal is first calculated. Then the interface temperature is obtained by averaging the local temperature around the interface. In the current work, unless otherwise specified, the temperature quoted refers to the interfacial temperature, which is determined by using the method described in refs 29, 34.

The temperature dependence of diffusion constant (D) of liquid Ni and Al is calculated. More specifically, a MD simulation is carried out on pure liquids at each temperature. For a given temperature, the mean-squared displacement (MSD) over each atom is calculated. The diffusion constant is directly calculated from the slope of the time evolution function of MSD. Figure 7 presents the plot of diffusion constant versus T , which can be well fitted by Arrhenius equation, namely $D = D_0 \exp(-Q/k_B T)$. Here k_B , Q and T are Boltzmann constant, the activation energy for diffusions and the temperature, respectively. And D_0 is a constant. By fitting to Arrhenius equation, we have obtained, $D_0 = 73.7 \pm 1.1 \times 10^9 \text{ m}^2/\text{s}$ (Al) and $59 \pm 1 \times 10^9 \text{ m}^2/\text{s}$ (Ni), $Q = 0.315 \pm 0.008 \text{ eV}$ (Al) and $0.510 \pm 0.007 \text{ eV}$ (Ni). By assuming the diffusion holding the same activation energy throughout the whole temperature region, the diffusion constants of liquid can be extrapolated by Arrhenius equation.

To calculate the defect concentration in the product crystal, we follow the method used previously³⁹. At the end of solidification, the product crystal is quenched to zero temperature using a steepest-descent algorithm to relax the atoms to their nearest local minimum. After this quenching, the atoms in the crystalline regions could be unambiguously assigned to the ideal crystal position. Then the real number of atoms in each crystal plane is counted, and defect concentrations are calculated. For each solidification process, before steady-state growth is

observed to set in, the system undergoes a transient behavior with an initial period of approximately several hundreds picosecond (ps), which is a common feature in the simulation of solidification²³. All the data and analysis are carried out on the crystal produced during steady-state growth.

Data Availability Statement. All relevant data are within the paper.

References

- Asta, M. *et al.* Solidification microstructures and solid-state parallels: Recent developments, future directions. *Acta Mater.* **57**, 941–971 (2009).
- Chernov, A. A. Notes on interface growth kinetics 50 years after Burton, Cabrera and Frank. *J. Cryst. Growth* **264**, 499–518 (2004).
- Rodway, G. H. & Hunt, J. D. Thermoelectric investigation of solidification of lead II. Lead alloys. *J. Cryst. Growth* **112**, 554–562 (1991).
- Broughton, J. Q., Gilmer, G. H. & Jackson, K. A. Crystallization rates of a Lennard-Jones liquid. *Phys. Rev. Lett.* **49**, 1496–1500 (1982).
- Burke, E., Broughton, J. Q. & Gilmer, G. H. Crystallization of fcc (111) and (100) crystal-melt interfaces: A comparison by molecular dynamics for the Lennard-Jones system. *J. Chem. Phys.* **89**, 1030–1041 (1988).
- Tymczak, C. J. & Ray, J. R. Asymmetric crystallization and melting kinetics in sodium: A molecular-dynamics study. *Phys. Rev. Lett.* **64**, 1278–1281 (1990).
- Tymczak, C. J. & Ray, J. R. Interface response function for a model of sodium: A molecular dynamics study. *J. Chem. Phys.* **92**, 7520–7530 (1990).
- Richardson, C. F. & Clancy, P. Picosecond laser processing of copper and gold. *Mol. Simul.* **7**, 335–355 (1991).
- Richardson, C. F. & Clancy, P. Contribution of thermal conductivity to the crystal-regrowth velocity of embedded-atom-method-modeled metals and metal alloys. *Phys. Rev. B* **45**, 12260 (1992).
- Moss, R. & Harrowell, P. Dynamic Monte Carlo simulations of freezing and melting at the 100 and 111 surfaces of the simple cubic phase in the face-centered-cubic lattice gas. *J. Chem. Phys.* **100**, 7630–7639 (1994).
- Briels, W. J. & Tepper, H. L. Crystal Growth of the Lennard-Jones (100) Surface by Means of Equilibrium and Nonequilibrium Molecular Dynamics. *Phys. Rev. Lett.* **79**, 5074–5077 (1997).
- Huitema, H. E. A., Vlot, M. J. & van der Eerden, J. P. Simulations of crystal growth from Lennard-Jones melt: Detailed measurements of the interface structure. *J. Chem. Phys.* **111**, 4714–4723 (1999).
- Huitema, H. E. A., Hengstum, Bvan & van der Eerden, J. P. Simulation of crystal growth from Lennard-Jones solutions. *J. Chem. Phys.* **111**, 10248–10260 (1999).
- Hoyt, J. J., Sadigh, B., Asta, M. & Foiles, S. M. Kinetic phase field parameters for the Cu-Ni system derived from atomistic computations. *Acta Mater.* **47**, 3181–3187 (1999).
- Celestini, F. & Debierre, J. M. Nonequilibrium molecular dynamics simulation of rapid directional solidification. *Phys. Rev. B* **62**, 14006–14011 (2000).
- Tepper, H. L. & Briels, W. J. Simulations of crystallization and melting of the FCC(100) interface: the crucial role of lattice imperfections. *J. Cryst. Growth* **230**, 270–276 (2001).
- Tepper, H. L. & Briels, W. J. Crystal growth and interface relaxation rates from fluctuations in an equilibrium simulation of the Lennard-Jones (100) crystal-melt system. *J. Chem. Phys.* **116**, 5186–5195 (2002).
- Celestini, F. & Debierre, J. M. Measuring kinetic coefficients by molecular dynamics simulation of zone melting. *Phys. Rev. E* **65**, 041605 (2002).
- Hoyt, J. J. & Asta, M. Atomistic computation of liquid diffusivity, solid-liquid interfacial free energy, and kinetic coefficient in Au and Ag. *Phys. Rev. B* **65**, 214106 (2002).
- Hoyt, J. J., Asta, M. & Karma, A. Atomic-scale simulation study of equilibrium solute adsorption at alloy solid-liquid interfaces. *Interface Sci.* **10**, 149–158 (2002).
- Jackson, K. A. The interface kinetics of crystal growth processes. *Interface Sci.* **10**, 159–169 (2002).
- Sun, D. Y., Asta, M. & Hoyt, J. J. Crystal-melt interfacial free energies and mobilities in fcc and bcc Fe. *Phys. Rev. B* **69**, 174103 (2004).
- Sun, D. Y., Asta, M. & Hoyt, J. J. Kinetic coefficient of Ni solid-liquid interfaces from molecular-dynamics simulations. *Phys. Rev. B* **69**, 024108 (2004).
- Hoyt, J. J., Asta, M. & Sun, D. Y. Molecular dynamics simulations of the crystal-melt interfacial free energy and mobility in Mo and V. *Philos. Mag.* **86**, 3651–3664 (2006).
- Xia, Z. G., Sun, D. Y., Asta, M. & Hoyt, J. J. Molecular dynamics calculations of the crystal-melt interfacial mobility for hexagonal close-packed Mg. *Phys. Rev. B* **75**, 012103 (2007).
- Ashkenazy, Y. & Averback, R. S. Atomic mechanisms controlling crystallization behaviour in metals at deep undercoolings. *Europhys. Lett.* **79**, 26005 (2007).
- Buta, D., Asta, M. & Hoyt, J. J. Atomistic simulation study of the structure and dynamics of a faceted crystal-melt interface. *Phys. Rev. E* **78**, 031605 (2008).
- Maltsev, I., Mirzoev, A., Danilov, D. & Nestler, B. Atomistic and mesoscale simulations of free solidification in comparison. *Modell. Simul. Mater. Sci. Eng.* **17**, 055006 (2009).
- Monk, J. *et al.* Determination of the crystal-melt interface kinetic coefficient from molecular dynamics simulations. *Modell. Simul. Mater. Sci. Eng.* **18**, 015004 (2010).
- Ashkenazy, Y. & Averback, R. S. Kinetic stages in the crystallization of deeply undercooled body-centered-cubic and face-centered-cubic metals. *Acta Mater.* **58**, 524–530 (2010).
- Mendelev, M. I., Rahman, M. J., Hoyt, J. J. & Asta, M. Molecular-dynamics study of solid-liquid interface migration in fcc metals. *Modell. Simul. Mater. Sci. Eng.* **18**, 074002 (2010).
- Wilson, S. R. & Mendelev, M. I. Dependence of solid-liquid interface free energy on liquid structure. *Modell. Simul. Mater. Sci. Eng.* **22**, 065004 (2014).
- Chan, W. L. & Averback, R. S. Anisotropic atomic motion at undercooled crystal/melt interfaces. *Phys. Rev. B* **82**, 020201 (2010).
- Gao, Y. F., Yang, Y., Sun, D. Y., Asta, M. & Hoyt, J. J. Molecular dynamics simulations of the crystal-melt interface mobility in HCP Mg and BCC Fe. *J. Cryst. Growth* **312**, 3238–3242 (2010).
- Zheng, X. Q., Yang, Y. & Sun, D. Y. Atomistic characterization of a modeled binary ordered alloy solid-liquid interface. *Acta Phys. Sin.* **62**, 017101 (2013).
- Fang, T., Wang, L. & Qi, Y. Molecular dynamics simulation of crystal growth of undercooled liquid Co. *Physica B* **423**, 6–9 (2013).
- Beckera, C. A., Asta, M., Hoyt, J. J. & Foiles, S. M. Equilibrium adsorption at crystal-melt interfaces in Lennard-Jones alloys. *J. Chem. Phys.* **124**, 164708 (2006).
- Kerrache, A., Horbach, J. & Binder, K. Molecular-dynamics computer simulation of crystal growth and melting in Al₅₀Ni₅₀. *Europhys. Lett.* **81**, 58001 (2008).
- Zheng, X. Q. *et al.* Disorder trapping during crystallization of the B2-ordered NiAl compound. *Phys. Rev. E* **85**, 041601 (2012).
- Kramer, M. J., Mendelev, M. I. & Napolitano, R. E. *In situ* observation of antisite defect formation during crystal growth. *Phys. Rev. Lett.* **105**, 245501 (2010).

41. Yang, Y. *et al.* Atomistic simulations of nonequilibrium crystal-growth kinetics from alloy melts. *Phys. Rev. Lett.* **107**, 025505 (2011).
42. Aziz, M. J. Model for solute redistribution during rapid solidification. *J. Appl. Phys.* **53**, 1158–1168 (1982).
43. Van Siclen, C. D. W. & Wolfer, W. G. Nonequilibrium vacancy entrapment by rapid solidification. *Acta Metall. Mater.* **40**, 2091–2100 (1992).
44. Aziz, M. J. & Boettinger, W. J. On the transition from short-range diffusion-limited to collision-limited growth in alloy solidification. *Acta Metall. Mater.* **42**, 527–537 (1994).
45. Boettinger, W. J. & Aziz, M. J. Theory for the trapping of disorder and solute in intermetallic phases by rapid solidification. *Acta Metall.* **37**, 3379–3391 (1989).
46. Boettinger, W. J., Bendersky, L. A., Cline, J., West, J. A. & Aziz, M. J. Disorder trapping in Ni₂TiAl. *Mater. Sci. Eng. A* **133**, 592–595 (1991).
47. Schwarz, M., Arnold, C. B., Aziz, M. J. & Herlach, D. M. Dendritic growth velocity and diffusive speed in solidification of undercooled dilute Ni-Zr melts. *Mater. Sci. Eng. A* **226–228**, 420–424 (1997).
48. Assadi, H., Reutzel, S. & Herlach, D. M. Kinetics of solidification of B2 intermetallic phase in the Ni-Al system. *Acta Mater.* **54**, 2793–2800 (2006).
49. Reutzel, S., Hartmann, H., Galenko, P. K., Schneider, S. & Herlach, D. M. Change of the kinetics of solidification and microstructure formation induced by convection in the NiAl system. *Appl. Phys. Lett.* **91**, 041913 (2007).
50. Hartmann, H., Holland-Moritz, D., Galenko, P. K. & Herlach, D. M. Evidence of the transition from ordered to disordered growth during rapid solidification of an intermetallic phase. *Europhys. Lett.* **87**, 40007 (2009).
51. Davidchack, R. L. & Laird, B. B. Simulation of the binary hard-sphere crystal/melt interface. *J. Chem. Phys.* **108**, 9452–9462 (1998).
52. Ercolessi, F. M. & Adams, J. B. Interatomic potentials from first-principles calculations: the force-matching method. *Europhys. Lett.* **26**, 583–588 (1994).
53. Foiles, S. M., Baskes, M. I. & Daw, M. S. Erratum: Embedded-atom-method functions for the fcc metals Cu, Ag, Au, Ni, Pd, Pt, and their alloys. *Phys. Rev. B* **33**, 7983 (1986).
54. Broughton, J. Q., Bonissent, A. & Abraham, F. F. The fcc (111) and (100) crystal-melt interfaces: A comparison by molecular dynamics simulation. *J. Chem. Phys.* **74**, 4029–4039 (1981).
55. Plimpton, S. Fast parallel algorithms for short-range molecular dynamics. *J. Comput. Phys.* **117**, 1–19 (1995).
56. Nosé, S. A unified formulation of the constant temperature molecular dynamics methods. *J. Chem. Phys.* **81**, 511–519 (1984).
57. Hoover, W. G. Canonical dynamics: equilibrium phase-space distributions. *Phys. Rev. A* **31**, 1695–1697 (1985).
58. Parrinello, M. & Rahman, A. Polymorphic transitions in single crystals: a new molecular dynamics method. *J. Appl. Phys.* **52**, 7182–7190 (1981).
59. Parrinello, M. & Rahman, A. Crystal structure and pair potentials: A molecular-dynamics study. *Phys. Rev. Lett.* **45**, 1196–1199 (1981).
60. Mendeleev, M. I., Schmalian, J., Wang, C. Z., Morris, J. R. & Ho, K. M. Interface mobility and the liquid-glass transition in a one-component system described by an embedded atom method potential. *Phys. Rev. B* **74**, 104206 (2006).
61. Morris, J. R., Mendeleev, M. I. & Srolovitz, D. J. A comparison of crystal-melt interfacial free energies using different Al potentials. *J. Non-Cryst. Sol.* **353**, 3565–3569 (2007).
62. Hoyt, J. J., Asta, M. & Karma, A. Method for computing the anisotropy of the solid-liquid interfacial free energy. *Phys. Rev. Lett.* **86**, 5530–5533 (2001).

Acknowledgements

This research is supported by the Natural Science Foundation of China (Grant No. 11174079), National Basic Research Program of China (973, Grant No. 2012CB921401), Shuguang and Innovation Program of Shanghai Education Committee. The computation is performed in the Supercomputer Center of ECNU.

Author Contributions

H.Y. Zhang and F. Liu carried out the theoretical calculations. H.Y. Zhang, Y. Yang and D.Y. Sun analyzed the data and wrote the main manuscript text. All authors discussed the results and commented on the manuscript.

Additional Information

Competing Interests: The authors declare that they have no competing interests.

Publisher's note: Springer Nature remains neutral with regard to jurisdictional claims in published maps and institutional affiliations.



Open Access This article is licensed under a Creative Commons Attribution 4.0 International License, which permits use, sharing, adaptation, distribution and reproduction in any medium or format, as long as you give appropriate credit to the original author(s) and the source, provide a link to the Creative Commons license, and indicate if changes were made. The images or other third party material in this article are included in the article's Creative Commons license, unless indicated otherwise in a credit line to the material. If material is not included in the article's Creative Commons license and your intended use is not permitted by statutory regulation or exceeds the permitted use, you will need to obtain permission directly from the copyright holder. To view a copy of this license, visit <http://creativecommons.org/licenses/by/4.0/>.

© The Author(s) 2017